Scripta Materialia 150 (2018) 66–69

Contents lists available at ScienceDirect

Scripta Materialia

journal homepage: www.elsevier.com/locate/scriptamat

Regular article

PdGe contact fabrication on Ga-doped Ge: Influence of implantation-mediated defects

T. Luo [a], J. Perrin Toinin [a], M. Descoins [a], K. Hoummada [a], M. Bertoglio [a], L. Chow [b], D. Narducci [c], A. Portavoce [a,*]

[a] IM2NP, CNRS/Aix-Marseille University, Faculté des Sciences de Saint-Jérôme case 142, 13397 Marseille, France
[b] Department of Physics, University of Central Florida, Orlando, FL 32816, USA
[c] Deprtament of Materials Science, University of Milano-Bicocca, via R. Cozzi 55, 20125 Milano, Italy

ARTICLE INFO

Article history:
Received 5 February 2018
Received in revised form 20 February 2018
Accepted 22 February 2018
Available online xxxx

Keywords:
Germanium
Palladium
Gallium
Contact
Reaction

ABSTRACT

PdGe contact fabrication on Ge(001) wafers doped with Ga is investigated using conventional complementary metal-oxide-semiconductor processes. Despite a p-type doping level of ~1.4×10^{20} cm^{-3}, the resistivity of the PdGe contact is found to be twice higher than that of undoped Ge. Ga doping has no influence on the Pd reaction with Ge. However, the doping process and the Salicide process led to the formation of Ga-Pd defects in both sides of the PdGe/Ge interface, resulting from Ga and Pd co-segregation on Ge dislocation loops.

So far, Ge has been mainly used alloyed with Si in microelectronics devices, allowing for example low power high-frequency devices to be produced at low cost [1]. However, devices made of pure Ge are currently gaining interest for microelectronics and optoelectronics applications [2,3]. Indeed, due to continuous device size reduction, Si needs to be replaced by other semiconductors in future devices [5]. Furthermore, the development of Si photonics requires optoelectronics device integration in the complementary metal-oxide-semiconductor (CMOS) technology [6]. Ge-based photodetectors are already integrated in Si photonics integrated circuits [6]. Current industrial Ge-based devices exhibit large sizes, as several roadblocks are still preventing Ge-based CMOS technology development. The two main issues concern i) high doping levels (>10^{20} at cm^{-3}) production [7,8], and ii) the fabrication of reliable ohmic contacts [9–11], especially concerning *n*-type Ge. The classical doping method in CMOS technology uses room-temperature dopant implantation followed by dopant activation via rapid thermal annealing (RTA) [12]. Ohmic contact fabrication on device's active zones in CMOS technology uses the 'Salicide' process based on the reaction of a thin metallic film with the semiconductor [13]. Ga is expected to be the ideal p-type dopant in Ge, as its solubility limit in Ge is close to 1 at.% [14] and its atomic diffusion kinetics is the slowest among the vacancy-mediated diffusing dopants [15,16]. PdGe is a serious candidate for ohmic contact production on Ge, since it exhibits a low resistivity, grows below 250 °C consuming a reduced amount of Ge, and is stable up to ~500 °C [9,17–19]. Consequently, combining high doping level and low contact resistivity, PdGe contact on Ga-doped Ge is expected to be a very promising solution for low-resistivity ohmic contact production on p-type Ge.

This work aimed to investigate the formation of a PdGe contact on implantation-mediated Ga-doped Ge(001) via the Salicide process. A 4-in. *n*-type Ge(001) substrate homogeneously doped with 1×10^{17} Sb at cm^{-3} was implanted with a Ga dose of 3.0×10^{15} at cm^{-2} using a beam energy of 80 keV, before being cut into several pieces in order to perform different measurements at different process steps sustained by the sample. After implantation, the sample was annealed under vacuum (~4×10^{-5} Torr) in a commercial RTA setup at 700 °C for 30 min in order to activate the Ga atoms. The Ga distribution in the Ge(001) substrate before and after activation was determined by secondary ion mass spectrometry (SIMS) using a CAMECA IMS 3F setup with a 3 keV O_2^+ ion beam, and the average Ga activation level was measured using Hall Effect measurements carried out at room temperature (RT) using a magnetic field of 0.5 T. A 20-nm thick polycrystalline Pd film was deposited on the sample surface at RT, using a commercial magnetron sputtering system with a base pressure of 10^{-8} Torr. Pd was sputtered from a 99.99% pure Pd target using a 99.9999% pure Ar gas flow in the DC mode. The reaction between the Pd layer and the Ge substrate allowing PdGe formation was investigated during X-ray diffraction (XRD) in situ annealing under vacuum (10^{-6} Torr) between RT and 400 °C. The annealing consisted of a heating ramp made of 5 °C per minute steps separated by 5 min-long XRD measurements at constant temperature (*T*), corresponding to an average ramp of ~1.7

* Corresponding author.
E-mail address: alain.portavoce@im2np.fr (A. Portavoce).

https://doi.org/10.1016/j.scriptamat.2018.02.037
1359-6462/

°C min^{-1}. The XRD measurements were performed in the Bragg-Brentano geometry using a Cu K_α source ($\lambda_{K\alpha} = 0.154$ nm). The atomic distributions in the sample both after the activation annealing at 700 °C, and after the ramp annealing up to 400 °C promoting Pd/Ge reaction, were determined by atom probe tomography (APT) using a CAMECA LEAP 3000X-HR system. The APT samples were prepared by focus ion beam (FIB) [20]. The measurements were performed in the laser mode at T ~23 K with a laser energy of 0.15 nJ, a laser pulse frequency of 100 kHz, and an average detection rate of 2 ions per 1000 laser pulses. Finally, the PdGe film resistivity (ρ) was measured using the four probe technique, and compared to the resistivity of a PdGe film grown in the same condition on the same Ge substrate but not implanted with Ga.

Fig. 1 presents the Ga SIMS profiles measured in the Ge(001) substrate after Ga implantation and after activation annealing. After implantation (dash line, open squares), the Ga concentration profile corresponds to a Gaussian distribution with a maximum concentration of ~5×10^{20} at cm^{-3} located at a depth of ~35 nm underneath the surface. After annealing at $T = 700$ °C for $t = 30$ min (solid line, solid squares), the Ga concentration profile is made of two distributions. The first one corresponds to immobile Ga atoms located close to the initial concentration maximum, and exhibiting a maximum concentration of ~3.5×10^{20} at cm^{-3}. The second one is due to Ga atoms that diffused in the Ge substrate during annealing under a concentration of ~1×10^{20} at cm^{-3}, with an average diffusion length l~85 nm, corresponding to a Ga diffusion coefficient D ~1.0×10^{-14} cm^2 s^{-1} according to $l^2 = 4Dt$. APT measurements (inset in Fig. 1) showed that immobile Ga atoms result from Ga segregation on dislocation loops (DLs) located at the depths 20 and 40 nm in the Ge substrate. The Ga accumulations (black iso-concentration surface in the inset of Fig. 1) observed in the APT volumes contain about 3 to 5 Ga at.% and exhibit an average thickness of ~2 nm, and an average diameter of ~5 nm. Similar atomic segregation on DLs has been observed for other elements in Si and Ge after dopant implantation and activation annealing [21–24]. Dopant implantation can lead to the semiconductor amorphization. In this case, activation annealing promotes semiconductor recrystallization, leaving DLs regularly distributed at the depth of the initial amorphous/crystal interface [25,26]. In Ge, in addition to amorphization, dopant implantation may also lead to the formation of a porous structure located at the surface of the wafer [27], explaining the formation of additional DLs located closer to the Ge substrate surface after recrystallization [26]. Ge

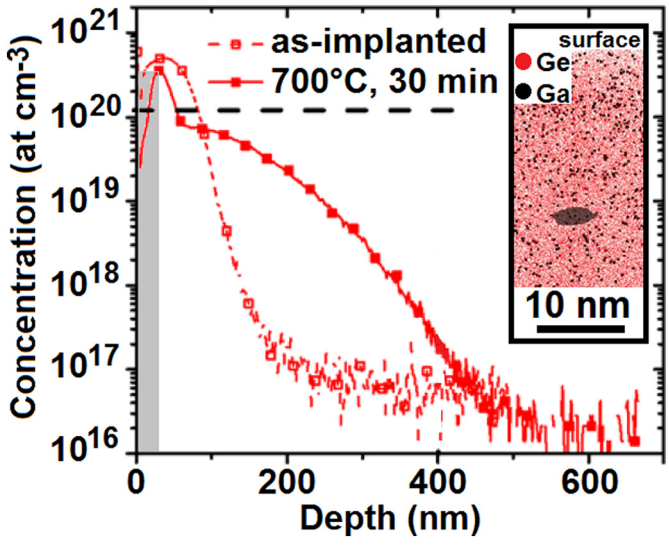

Fig. 1. Ga SIMS profiles measured in the Ge(001) substrate after Ga implantation before (dash line, open squares) and after (solid line, solid squares) activation annealing at 700 °C for 30 min. The gray region shows the Ge thickness consumed later-on to form the PdGe contact. The insert presents APT data obtained on the Ge substrate after Ga activation: red and black dots correspond to Ge and Ga atoms, respectively, and the black volume is delimited by a 3 Ga at.% iso-concentration surface.

recrystallization during activation annealing is in agreement with the fact that D is found to be about one order of magnitude higher than the Ga diffusion coefficient $D_{Ga}(700\ °C) = 1 \times 10^{-15}$ cm^2 s^{-1} reported in the literature [15], meaning that the apparent diffusion length determined from the Ga SIMS profiles in Fig. 1 does not correspond to Ga equilibrium diffusion, but to atomic transport during Ge crystallization [28]. Hall Effect measurements found an average hole concentration in the sample of ~1.4×10^{20} cm^{-3} after Ga activation (horizontal dash line in Fig. 1), which corresponds to a Ge resistivity of ~4.62×10^2 μΩ cm [29]. Fig. 2 displays the evolution of the X-ray diffractogram measured on this sample, after the deposition of a 20 nm-thick Pd layer at RT, during in situ annealing. After Pd deposition, only the Pd(111) diffraction peak was detected at the diffraction angle 2θ–40°. The intensity of this peak started to decrease at T ~140 °C, when the Pd_2Ge(111) and Pd_2Ge(002) diffraction peaks appeared at 2θ–37.5° and 53.7°, respectively. After the complete vanishing of the Pd diffraction peak, several PdGe diffraction peaks appeared at T ~200 °C. During the simultaneous decrease of the Pd_2Ge peak intensities, the intensity of the PdGe peaks (101), (111), (211), (121), and (002), corresponding respectively to 2θ–29.3°, 33.2°, 41.7°, 43°, and 52.5°, increased up to a maximum, which is reached once the Pd_2Ge phase is no longer detectable. Only PdGe diffraction peaks were detected at the end of the XRD in situ annealing. The Pd/Ge reaction led to the sequential formation of Pd_2Ge and PdGe, the phase sequence, the detected diffraction peaks, as well as the temperatures at which the two phases show up being similar to that of Pd reaction with intrinsic Ge(001) substrates [18,19,30]. The resistivity of the PdGe contact formed on Ga-doped Ge(001) was found to be ρ ~27 ± 1 μΩ cm, which is about twice the value measured on intrinsic Ge (ρ ~13 ± 1 μΩ cm). This result is quite surprising, especially in view of the doping level of ~1.4×10^{20} at $^{-3}$. Fig. 3a shows a sample volume analyzed by APT. An abrupt interface is observed between the germanide and the Ge substrate, as well as randomly distributed Ga atoms. However, Ga accumulations are also observed at both sides of the germanide/Ge interface (arrow in Fig. 3a). These Ga accumulations are disc-shaped, similar to those observed in Ge after Ga activation annealing. Ge, Pd, and Ga concentration profiles measured in the sample volume shown in Fig. 3a are reported in Fig. 3b. The composition of the germanide layer is homogeneous and corresponds to the PdGe stoichiometry. Ga atoms are detected both in the PdGe layer and in the Ge substrate, with a maximum concentration of ~0.5 at.% (~2.2×10^{20} at cm^{-3}) near the PdGe/Ge interface, where the Ga accumulations are present. Ga concentration in PdGe is ~0.08 at.% (~3.5×10^{19} at cm^{-3}), and a Ga concentration plateau of ~0.14 at.% (~6.2

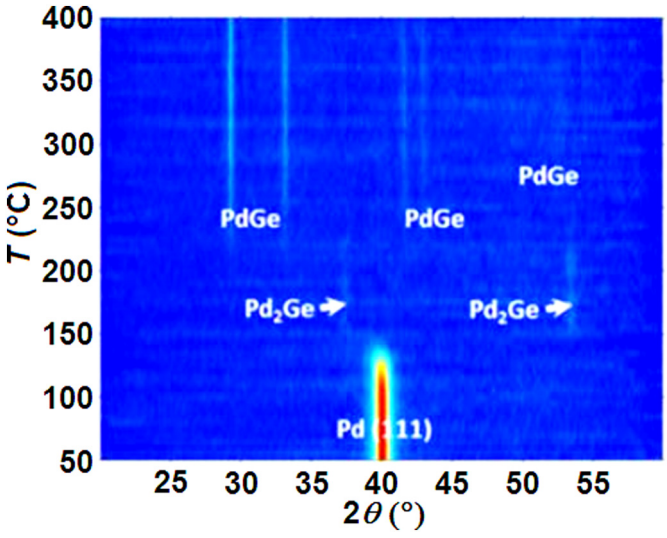

Fig. 2. In situ XRD measurements performed during Pd/Ge reaction between 50 and 400 °C, at an average heating ramp of 1.7 °C per minute.

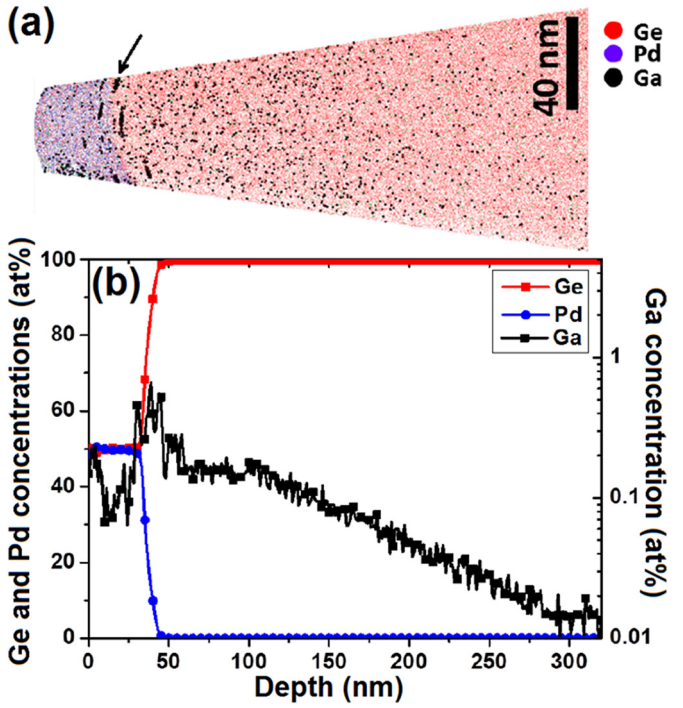

Fig. 3. APT measurements performed after Pd/Ge reaction promoted by an average temperature ramp of 1.7 °C per minute from RT to 400 °C: (a) side view of a sample volume (red, blue, and black dots corresponds to Ge, Pd, and Ga atoms, respectively), and (b) Ge (red squares, left axis), Pd (blue circles, left axis), and Ga (black squares, right axis) concentration profiles measured in the volume presented in (a).

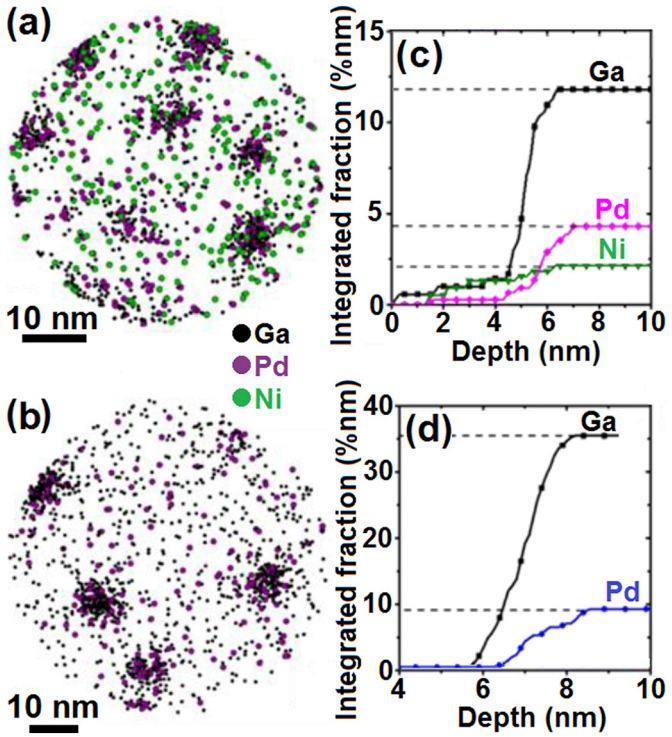

Fig. 4. APT measurements performed in volumes taken close to the PdGe/Ge interface in the sample volume presented in Fig. 3a, either in the PdGe film ((a) and (c)) or in the Ge substrate ((b) and (d)). (a) and (b) present the top-view of 5 nm-thick volumes (black, purple, and green dots correspond to Ga, Pd, and Ni atoms, respectively); (c) and (d) show Ga, Pd, and Ni integrated profiles.

$\times 10^{19}$ at cm^{-3}) is observed at a Ge substrate depth of 60–100 nm, along with a diffusion tail extending from 100 nm to ~300 nm, where the APT detection limit is reached (~10^{19} at cm^{-3}). The Ga profile measured by APT in Ge agrees with the Ga SIMS profile measured before Pd/Ge reaction. The Ga distribution in the Ge substrate was not significantly modified by the reaction. Indeed, the reaction of a 20 nm-thick Pd film with Ge is expected to consume 32 nm of Ge to form a 47 nm-thick PdGe layer [17,31]. The Ge thickness used to form the PdGe layer is represented by the gray region in Fig. 1, predicting the PdGe/Ge interface location at the Ga maximum concentration, in accordance with APT analyses. The depth of 32 nm is precisely located between the two distributions of DLs decorated with Ga atoms observed in the Ga-doped Ge substrate after activation annealing. Fig. 4a and b present atomic distributions observed in 5 nm-thick APT volumes extracted from the two sides of the PdGe/Ge interface in the APT volume shown in Fig. 3a. Only Ga (black dot), Pd (purple dot), and Ni (green dot) atoms are displayed in top view. The Ni atoms come from the Ni cap used to protect the sample during FIB sample preparation for APT experiments [20]. Ni atoms from this protection cap have been observed to segregate on DLs resulting from dopant implantation and activation processes in Si and Ge [23,24], since Ni can diffuse in Si and Ge at RT by the interstitial mechanism [32,33]. The two volumes in Fig. 4a and b show Ga atom accumulations in PdGe and Ge, exhibiting similar lateral sizes (~5–10 nm) and thicknesses (~2 nm). The integrated profiles [34] of the different elements, calculated through the clusters located in PdGe and Ge (Fig. 4c and d) allow the segregated concentration of the different elements to be determined. In PdGe, the Ga accumulations contain ~5 at.% of Ga, as well as ~2 at.% of Pd, and ~1 at.% of Ni. Furthermore, these clusters are surrounded by an important concentration of dissolved Ni and Pd atoms. In Ge, Ga accumulations contain ~18 at.% of Ga and ~5 at.% of Pd. No dissolved Pd or Ni atoms are detected surrounding the clusters, in agreement with the very low solubility limit of Pd and Ni in Ge [14]. The Ga cluster location and shape correspond to that of the implantation-mediated DLs decorated with Ga atoms observed in the Ge substrate before the reaction with Pd. Similar to Ni, Pd also uses the interstitial mechanism to diffuse in monocrystalline Ge [35,36]. Thus, as observed for Ni [24], after deposition of the 20 nm-thick Pd layer on the Ga-doped Ge substrate, Pd diffused at RT in Ge and co-segregated with Ga on the DLs located ~20 nm-deep and 40 nm-deep under the Pd/Ge interface. During the reaction between the Pd film and Ge, most of the segregated Ga and Pd atoms were immobile, and Ga and Pd atoms segregated on the DLs located 20 nm-deep in Ge were incorporated in PdGe, due to the consumption of ~32 nm of Ge. In this case, although the shape of the defects was similar to that of decorated DLs, the defects probably correspond to Ga-Pd clusters, since Ga forms several compounds with Pd [14,37]. In Ge, the Ga-Pd accumulations initially located 40 nm-deep in Ge are expected to still correspond to Ge DLs decorated with Ga and Pd atoms. However, one can note that after PdGe growth, Ga accumulations in Ge were found to have a lateral size two times larger (~10 nm) and Ga concentrations about ~4.5 times higher, suggesting that i) DLs grew during Pd/Ge reaction due to Ge self-interstitial injection, as observed during the growth of several silicides [38,39], and ii) Ga atoms may have been more mobile near the growing DLs. Finally, when the sample was prepared for APT measurements, a Ni cap was deposited on the PdGe film surface, and Ni could diffuse in the polycrystalline PdGe layer, and accumulate near the Ga-Pd clusters located in this layer.

In summary, Ga implantation followed by Ga activation annealing promoted the formation of Ga-decorated DLs distributed close to the maximum of the implanted Ga distribution. Subsequent Pd deposition on the sample surface allowed Pd atoms to co-segregate with Ga on the DLs located in the Ge substrate. Part of these defects was finally incorporated in the PdGe contact during its fabrication via the Salicide process. The presence of such defects in both sides of the PdGe/Ge interface significantly deteriorated the contact properties, despite the significant Ga doping level reached in Ge before germanidation.

This work was supported by the French National Agency for Research (ANR) through the program “Science de l'ingénierie” (Project DoGeTec, no. ANR-12-JS09-0015-1).

References

[1] K. Washio, in: Y. Shiraki, N. Usami (Eds.), Silicon–Germanium (SiGe) Nanostructures, Woodhead Publishing, Oxford 2011, p. 473 (Part IV).
[2] S. Takagi, S.-H. Kim, M. Yokoyama, R. Zhang, N. Taoka, Y. Urabe, T. Yasuda, H. Yamada, O. Ichikawa, N. Fukuhara, M. Hata, M. Takenaka, Solid State Electron. 88 (2013) 2.
[3] D. Thomson, A. Zilkie, J.E. Bowers, T. Komljenovic, G.T. Reed, L. Vivien, D. Marris-Morini, E. Cassan, L. Virot, J.-M. Fédéli, J.-M. Hartmann, J.H. Schmid, D.-X. Xu, F. Boeuf, P. O'Brien, G.Z. Mashanovich, M. Nedeljkovic, J. Opt. 18 (2016), 073003. .
[5] S. Ghosh, P. Bhatt, Y. Tiwari, C. Joishi, S. Lodha, J. Appl. Phys. 120 (2016), 095703. .
[6] S. Nagatomo, Y. Ishikawa, J. Vac. Sci. Technol., B: Nanotechnol. Microelectron.: Mater., Process., Meas., Phenom. 35 (2017), 051206. .
[7] E. Simoen, M. Schaekers, J. Liu, J. Luo, C. Zhao, K. Barla, N. Collaert, Phys. Status Solidi A (2016) 1.
[8] R. Milazzo, G. Impellizzeri, D. Piccinotti, A. La Magna, G. Fortunato, D. De Salvador, A. Carnera, A. Portavoce, D. Mangelinck, V. Privitera, E. Napolitani, J. Appl. Phys. 119 (2016), 045702. .
[9] J. Perrin Toinin, K. Hoummada, M. Bertoglio, A. Portavoce, Scr. Mater. 120 (2016) 45.
[10] D. Biswas, J. Biswas, S. Ghosh, B. Wood, S. Lodha, Appl. Phys. Lett. 110 (2017), 052104. .
[11] D. Vaidya, S. Lodha, S. Ganguly, J. Appl. Phys. 121 (2017) 145701.
[12] J. Bhandari, M. Vinet, T. Poiroux, B. Previtali, B. Vincent, L. Hutin, J.P. Barnes, S. Deleonibus, A.M. Ionescu, Mater. Sci. Eng. B 154–155 (2008) 114.
[13] A. Lauwers, J.A. Kittl, M.J.H. Van Dal, O. Chamirian, M.A. Pawlak, M. de Potter, R. Lindsay, T. Raymakers, X. Pages, B. Mebarki, T. Mandrekar, K. Maex, Mater. Sci. Eng. B 114–115 (2004) 29.
[14] A. Gokhale, G.J. Abbaschian, Binary Alloy Phase Diagrams, 2nd ed. ASM International, 1990.
[15] S. Uppal, A. Willoughby, J. Bonar, N. Cowern, T. Grasby, J. Appl. Phys. 96 (2004) 1376.
[16] C. Chui, L. Kulig, J. Moran, W. Tsai, K. Saraswat, Appl. Phys. Lett. 87 (2005), 091909. .
[17] S. Gaudet, C. Detavernier, A. Kellock, P. Desjardins, C. Lavoie, J. Vac. Sci. Technol. A 24 (2006) 1474.
[18] J. Perrin Toinin, K. Hoummada, M. Bertoglio, A. Portavoce, Scr. Mater. 122 (2016) 22.
[19] M. Descoins, J. Perrin Toinin, S. Zhiou, K. Hoummada, M. Bertoglio, R. Ma, L. Chow, D. Narducci, A. Portavoce, Scr. Mater. 139 (2017) 104.
[20] A. Portavoce, K. Hoummada, A. Ronda, D. Mangelinck, I. Berbezier, J. Beilstein, Nanotechnology 5 (2014) 2374.
[21] K. Thompson, P.L. Flaitz, P. Ronsheim, D.J. Larson, T.F. Kelly, Science 317 (2007) 1370.
[22] S. Duguay, T. Philippe, F. Cristiano, D. Blavette, Appl. Phys. Lett. 97 (2010), 242104. .
[23] K. Hoummada, D. Mangelinck, B. Gault, M. Cabié, Scr. Mater. 64 (2011) 378.
[24] J. Perrin Toinin, A. Portavoce, M. Texier, M. Bertoglio, K. Hoummada, Appl. Phys. Lett. 108 (2016), 232103. .
[25] A. Claverie, S. Koffel, N. Cherkashin, G. Benassayag, P. Scheiblin, Thin Solid Films 518 (2010) 2307.
[26] J. PerrinToinin, A. Portavoce, K. Hoummada, M. Texier, M. Bertoglio, S. Bernardini, L. Chow, Mater. Sci. Semicond. Process. 42 (2016) 215.
[27] G. Impellizzeri, S. Mirabella, A. Irrera, M.G. Grimaldi, E. Napolitani, J. Appl. Phys. 106 (2009), 013518. .
[28] A. Portavoce, R. Simola, D. Mangelinck, J. Bernardini, P. Fornara, Diffus. Defect Data 264 (2007) 33.
[29] D.B. Cuttriss, Bell Syst. Tech. J. (1961) 509.
[30] F.A. Geenen, W. Knaepen, K. De Keyser, K. Opsomer, R.L. Vanmeirhaeghe, J. Jordan-Sweet, C. Lavoie, C. Detavernier, Thin Solid Films 551 (2014) 86.
[31] V. Ignatkov, V. Kosenko, Sov. Phys. Solid State 4 (1962) 11193.
[32] F. Van der Maesen, J.A. Brenkman, Philips Res. Rep. 9 (1954) 225.
[33] H. Bracht, S. Brotzmann, Mater. Sci. Semicond. Process. 9 (2006) 471.
[34] P. Maugis, K. Hoummada, Scr. Mater. 120 (2016) 90.
[35] H. Tahini, A. chroneos, S. Middleburgh, R. Schwingen-schögl, J. Mater. Chem. A 3 (2015) 13822.
[36] A. Chroneos, R. Vovk, J. Mater. Sci. Mater. Electron. 26 (2015) 13787–13789.
[37] K. Schubert, H. Breimer, W. Burkhardt, E. Grunzel, R. Haufler, H. Lukas, H. Vetter, J. Wegst, M. Wilkens, Naturwissenshaften 44 (1959) 1229–1230.
[38] M. Ronay, R.G. Schad, Phys. Rev. Lett. 64 (1990) 2042.
[39] J.E. Masse, P. Knauth, P. Gas, A. Charaï, J. Appl. Phys. 77 (1995) 934.